



## Receding-horizon optimal control of the current profile evolution during the ramp-up phase of a tokamak discharge

Y. Ou<sup>a,b,\*</sup>, C. Xu<sup>a,c</sup>, E. Schuster<sup>a</sup>, J.R. Ferron<sup>d</sup>, T.C. Luce<sup>d</sup>, M.L. Walker<sup>d</sup>, D.A. Humphreys<sup>d</sup>

<sup>a</sup> Department of Mechanical Engineering and Mechanics, Lehigh University, Bethlehem, PA 18015, USA

<sup>b</sup> Shenzhen Institutes of Advanced Technology, Chinese Academy of Sciences, Shenzhen, Guangdong 518055, China

<sup>c</sup> Department of Control Science & Engineering, Zhejiang University, Hangzhou, Zhejiang 310027, China

<sup>d</sup> DIII-D tokamak, General Atomics, San Diego, CA 92121, USA

### ARTICLE INFO

#### Article history:

Received 25 August 2009

Accepted 24 August 2010

Available online 25 September 2010

#### Keywords:

Current profile control

Receding horizon control

Tokamaks

### ABSTRACT

The control of the toroidal current density spatial profile in tokamak plasmas will be absolutely critical in future commercial-grade reactors to enable high fusion gain, non-inductive sustainment of the plasma current for steady-state operation, and magnetohydrodynamic (MHD) instability-free performance. The evolution in time of the current profile is related to the evolution of the poloidal magnetic flux, which is modeled in normalized cylindrical coordinates using a partial differential equation (PDE) usually referred to as the magnetic flux diffusion equation. The control objective during the ramp-up phase is to drive an arbitrary initial profile to approximately match, in a short time windows during the early flattop phase, a predefined target profile that will be maintained during the subsequent phases of the discharge. Thus, such a matching problem can be treated as an optimal control problem for a PDE system. A distinctive characteristic of the current profile control problem in tokamaks is that it admits interior, boundary and diffusivity actuation. A receding-horizon control scheme is proposed in this work to exploit this unique characteristic and to solve the associated open-loop finite-time optimal control problem using different optimization techniques. The efficiency of the proposed scheme is shown in simulations.

© 2010 Elsevier Ltd. All rights reserved.

## 1. Introduction

The need for new sources of energy is expected to become a critical problem within the next few decades. It is a fact that fossil fuel energy is becoming more expensive and polluting. Nuclear fission and fusion are candidate sources of energy with sufficient energy density to supply the increasing world population with its steadily increasing energy demands. In both fission and fusion reactions the total masses after the reaction are less than those before. The “lost” mass appears as energy, with the amount given by the famous Einstein formula,  $E = (M_r - M_p)c^2$ , where  $E$  is the energy,  $M_r$  is the mass of the reactant nuclei,  $M_p$  is the mass of the product nuclei, and  $c$  is the speed of light. In a fission reaction, a heavy nucleus splits apart into smaller nuclei. Fission is a mature technology powering present nuclear power reactors. In a fusion reaction, on the contrary, two light nuclei (deuterium and tritium (two isotopes of hydrogen)) stick together to form a heavier nucleus (helium) plus an energetic neutron. Like fission, fusion produces no air pollution or greenhouse gases, since the reaction product is helium. Unlike fission, fusion poses no risk of nuclear

accident, generation of high-level nuclear waste, and production of material for nuclear weapons. In addition, there is an abundant fuel supply. Deuterium, may be readily extracted from ordinary water, which is available to all nations. Tritium does not occur naturally but would be produced from lithium (through a nuclear reaction that makes use of the neutron resulting from the D–T fusion process), which is available from land deposits or from sea water which contain thousands of years’ supply. The world-wide availability of these materials would thus eliminate international tensions caused by imbalance in fuel supply.

Since nuclei carry positive charges, they normally repel one another when trying to fuse. To overcome the Coulomb barrier, the kinetic energy of the nuclei must be increased by heating. The fusion process requires extremely high temperatures (50–200 million Kelvin), at which the hydrogen gas ionizes and becomes a plasma. Within a plasma, electrons are free to move independently of the nucleus and the gas is essentially a sea of charged particles, which conduct electricity and interact with magnetic fields. One of the most promising approaches to fusion is indeed the magnetic confinement concept, which exploits these properties of the plasma. Strong magnetic fields act like a magnetic bottle to hold the ionized (charged) nuclei together and away from the vessel wall as they are heated to fusion temperatures. A Russian design in the shape of a torus, called

\* Corresponding author.

E-mail address: [yoo205@lehigh.edu](mailto:yoo205@lehigh.edu) (Y. Ou).

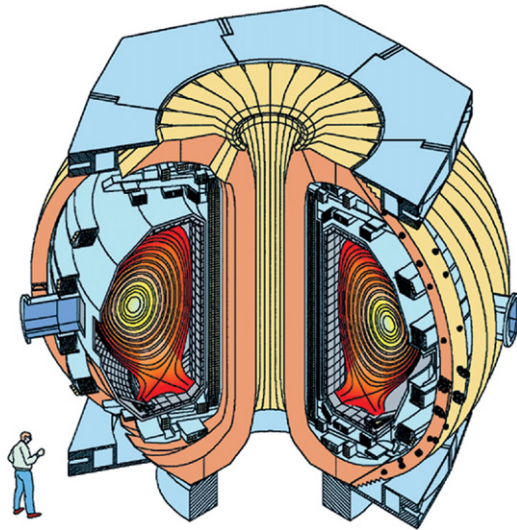


**Fig. 1.** Scheme of the DIII-D Tokamak. The toroidal field (TF) coils (creamy yellow) are wrapped “poloidally” around the torus (the short way, going through the center hole), while the poloidal field (PF) coils (light blue) are wrapped “toroidally” (the long way) around the torus. Current flowing in these conducting coils produces the helical magnetic field that confines the plasma. The plasma contained within the device is represented by a set of nested contours of constant magnetic flux. (For interpretation of the references to color in this figure legend, the reader is referred to the web version of this article.)

tokamak (Fig. 1), has proved particularly well suited for containing a fusion reaction. A more in-depth introduction to fusion can be found in Leuer (1995), Pironti and Walker (2005), Walker et al. (2006) and Schuster and Ariola (2006), in which considerable effort was made to describe the current problems of tokamak plasma control at a level that is accessible to engineers, mathematicians, and non-plasma physicists.

In a tokamak (Fig. 1), the magnetic field lines twist their way around the torus to form a helical structure. The toroidal magnetic field component is produced by the so-called “toroidal field” (TF) coils. Addition of a poloidal magnetic field component, generated by the toroidal plasma current and the “poloidal field” (PF) coils, is necessary for the existence of a magnetohydrodynamic (MHD) equilibrium (Freidberg, 1987). It is possible to use the poloidal component of the helicoidal magnetic lines to define nested toroidal surfaces corresponding to constant values of the poloidal magnetic flux. The poloidal flux  $\psi$  at a point  $P$  is the total flux through the surface  $S$  bounded by the toroidal ring passing through  $P$ , i.e.,  $\psi = \int B_{pol} dS$ . The dynamics of the poloidal magnetic flux is governed by a parabolic partial differential equation (PDE) usually referred to as the magnetic flux diffusion equation. The shape of the poloidal magnetic flux profile has a direct effect on the current density profile since they are related by spatial derivative operations.

The need to optimize the tokamak concept for the design of an economical, possibly steady state, fusion power plant have motivated extensive international research aimed at finding the so-called “advanced tokamak (AT) operation scenarios” (Taylor, 1997). In a large number of machines, experiments have demonstrated the existence of such regimes characterized by a high confinement state with improved MHD stability, which yields a strong increase of the plasma performance quantified by the normalized energy confinement time and plasma pressure. In such conditions a dominant fraction of the plasma current is self-generated by the neo-classical bootstrap mechanism, which alleviates the requirement on externally driven current and enables steady-state operation. This highly confined state is achieved to a large extent by the generation of a so-called

“internal transport barrier” (ITB) (Connor et al., 2004), a region where the plasma turbulence (and therefore the plasma transport) is almost suppressed. Many studies have shown the key influence of the current density profile on triggering the ITBs (Challis, 2004). This provides a strong motivation for the control of the current density profile in real time.

Recent experiments in different devices around the world (JET, (Laborde et al., 2005; Moreau et al., 2003, 2008), DIII-D (Ferron et al., 2006), JT-60U (Suzuki et al., 2005), Tore Supra (Barana, Mazon, Laborde, & Turco, 2007; Wijnands et al., 1997) have demonstrated significant progress in achieving profile control. At JET, different current and temperature gradient target profiles have been reached and sustained for several seconds during the flat-top current phase. The control schemes rely on the experimental identification of linearized static (Laborde et al., 2005; Moreau et al., 2003) and dynamic (Moreau et al., 2008) response models, using lower hybrid current drive (LHCD), ion cyclotron resonance heating (ICRH) and neutral beam injection (NBI) as actuators. The controllers, which finally reduce to proportional-integral regulators incorporating information of the identified response of the system and exploiting the different time scales of kinetic and magnetic variables, have been proved effective in experiments. Experiments at DIII-D (Ferron et al., 2006) focus on creating the desired current density profile during the plasma current ramp-up and early flat-top phases with the aim of maintaining this target profile during the subsequent phases of the discharge. Since the actuators that are used to achieve the desired target profile are constrained, experiments have shown that some of the desirable target profiles may not be achieved for all arbitrary initial conditions. Therefore, a perfect matching of the desirable target profile may not be physically possible. In practice, the objective is to achieve the best possible approximate matching in a short time windows  $[T_1, T_2]$  during the early flat-top phase of the total plasma current pulse, as shown in Fig. 2. Thus, such a matching problem can be treated as a finite-time optimal control problem for a parabolic PDE system.

The control of the current density profile in tokamak plasmas is unique in the sense that it admits actuation not only through interior control (see, e.g., Christofides, 2001 and references therein) and boundary control (see, e.g., Krstic & Smyshlyayev, 2008 and references therein) but also through what is named

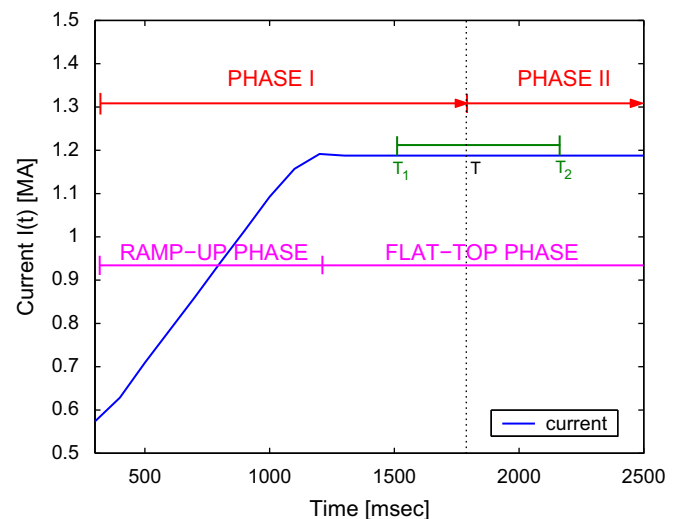


**Fig. 2.** The total plasma current evolution can be roughly divided into two phases: the ramp-up phase and the flat-top phase. The control problem focuses on phase I that includes the ramp-up phase and the first part of the flat-top phase. The control goal is to drive the current profile from some initial arbitrary condition to a predefined target profile at some time  $T$  between the time window  $[T_1, T_2]$ , which is in the flat-top phase.

diffusivity control (plasma resistivity) in this paper. Exploiting these actuation capabilities, previous work by the authors includes the investigation of the use of extremum seeking (Ou et al., 2008) and nonlinear programming (Xu et al., 2010) to achieve open-loop solutions for the optimal control problem defined during the ramp-up and early flat-top phases. The time evolutions of the control inputs are obtained in the interval  $[0, T]$  in order to minimize the quadratic error between actual and desired current profiles at time  $T$  (see Fig. 2). The work is aimed at saving long trial-and-error periods of time currently spent by fusion experimentalists trying to manually adjust the time evolutions of the actuators to achieve the desired current profile at some time  $T$  within a prespecified window  $[T_1, T_2]$ . However, these open-loop solutions are very sensitive to disturbances and uncertainties.

In this paper this limitation is overcome by proposing a receding-horizon control strategy for the current profile control problem in tokamak plasmas. The term receding horizon control (RHC) describes a class of algorithms that at each control interval compute an open-loop sequence of manipulated input variables in order to optimize the future behavior of the plant over a specific time horizon. In the last two decades, several formulations have been developed for linear and nonlinear systems (Findeisen & Allgower, 2002; Mayne & Michalska, 1990; Mayne, Rawlings, Rao, & Scokaert, 2000) finding many successful applications, particularly in the process industry (Marjanovic & Lennox, 2004; Richalet, 1993) but also in other areas (Borrelli, Falcone, & Vecchio, 2007; Keviczky & Balas, 2006; Kim, Yoon, & Kwon, 2001; van Straten, van Willigenburg, & Tap, 2002). The use of RHC schemes for the control of PDE systems is part of the literature in this field (Bleis & Kothare, 2005; Dubljevic, El-Farra, Mhaskar, & Christofides, 2006; Irizarry-Rivera & Seideer, 1997; Patwardhan, Wright, & Edgar, 1992; Toure, Biston, & Gilles, 1994). In this work, extremum seeking (Ariyur & Krstic, 2003) and nonlinear programming (Nocedal & Wright, 2006) techniques are used at each control interval to solve the associated optimization problem.

This paper is organized as follows. In Section 2, an infinite-dimensional dynamic model for the poloidal flux  $\psi$  is introduced. Section 3 describes the control objectives during the different phases of the tokamak discharge, and states the control problem. In Section 4, a closed-loop, receding-horizon approach is proposed for the solution of a finite-time optimal problem defined for the nonlinear distributed parameter system introduced in Section 2, which accepts diffusivity, interior, and boundary actuation. A simulation study showing the effectiveness of the proposed closed-loop controller is presented in Section 5. Finally, conclusions and identified future work are presented in Section 6.

## 2. Current profile evolution model

Let  $\rho$  be an arbitrary coordinate indexing the magnetic surface. Any quantity constant on each magnetic surface could be chosen as the variable  $\rho$ . The mean geometric radius of the magnetic surface is chosen as the variable  $\rho$ , i.e.,  $\pi B_{\phi,0} \rho^2 = \Phi$ , where  $\Phi$  is the toroidal magnetic flux and  $B_{\phi,0} = 1.85$  T is the reference toroidal magnetic field at the geometric plasma center  $R_0 = 1.67$  m. The variable  $\hat{\rho}$  denotes the normalized radius  $\rho/\rho_b$ , and  $\rho_b = 0.79$  m is the radius of the last closed flux surface. The evolution of the poloidal flux in normalized cylindrical coordinates is given by the magnetic diffusion equation (Ou et al., 2007),

$$\frac{\partial \psi}{\partial t} = \frac{\eta(T_e)}{\mu_0 \rho_b^2 \hat{F}^2 \hat{\rho}} \frac{\partial}{\partial \hat{\rho}} \left( \hat{\rho} \hat{F} \hat{G} \hat{H} \frac{\partial \psi}{\partial \hat{\rho}} \right) - R_0 \hat{H} \eta(T_e) \frac{\langle \bar{J}_{NI} \cdot \bar{B} \rangle}{B_{\phi,0}}, \quad (1)$$

where  $t$  is the time,  $\psi$  is the poloidal magnetic flux,  $\eta$  is the plasma resistivity,  $T_e$  is the plasma electron temperature,  $\mu_0 = 4\pi \times$

$10^{-7}$  H/m is the vacuum permeability,  $\bar{J}_{NI}$  is the non-inductive source of current density (neutral beam, electron cyclotron, etc.),  $\bar{B}$  is the toroidal magnetic field, and  $\langle \cdot \rangle$  denotes flux-surface average.  $\hat{F}, \hat{G}, \hat{H}$  are geometric factors, which are functions of  $\hat{\rho}$  and are depicted in Fig. 3. The boundary conditions are given by

$$\left. \frac{\partial \psi}{\partial \hat{\rho}} \right|_{\hat{\rho}=0} = 0, \quad \left. \frac{\partial \psi}{\partial \hat{\rho}} \right|_{\hat{\rho}=1} = \frac{\mu_0 R_0}{2\pi \hat{G}|_{\hat{\rho}=1} \hat{H}|_{\hat{\rho}=1}} I(t), \quad (2)$$

where  $I(t)$  denotes the total plasma current.

The model makes the simplifying assumption that the magnetic geometry is fixed in time. This excludes two potential sources of flux—a change in  $\rho_b$  (either by a change in the shape of the last closed flux surface or in  $B_{\phi,0}$ ) and a change in location of the geometric center of the interior flux surfaces relative to that of the last closed flux surface. Changes in  $\rho_b$  are small by design in the experiments of interest, but it is straightforward to include this effect in the model for situations where it would be important. Changes in the relative positions of the flux surfaces do occur, but for cases of interest, these happen slowly enough and they can be neglected.

During “Phase I” (see Fig. 2), mainly governed by the ramp-up phase, the plasma current is mostly driven by induction. In this case, it is possible to decouple the equation for the evolution of the poloidal flux from the evolution equation for the temperature  $T_e(\hat{\rho}, t)$ . Highly simplified models for the temperature and non-inductive toroidal current density are chosen for this phase. Based on experimental observations at DIII-D, the shapes of the profiles are assumed to remain fixed and equal to the so-called reference profiles, which are identified from DIII-D discharges associated with the experiment of interest (Ou et al., 2007). The responses to the actuators are simply scalar multiples of the reference profiles.

The temperature  $T_e$  is assumed to follow  $I(t)\sqrt{P_{tot}}/\bar{n}(t)$ , and can be written as

$$T_e(\hat{\rho}, t) = k_{Te} T_e^{profile}(\hat{\rho}) \frac{I(t)\sqrt{P_{tot}}}{\bar{n}(t)}, \quad (3)$$

where  $T_e^{profile}$  is given in Fig. 4,  $k_{Te} = 1.7295 \times 10^{10} \text{ m}^{-3} \text{ A}^{-1} \text{ W}^{-1/2}$ , and  $P_{tot}$  is the total power of the non-inductive current sources (electron cyclotron heating (ECH), neutral beam heating (NBH), etc.). The line-averaged plasma density is denoted by  $\bar{n}$ .

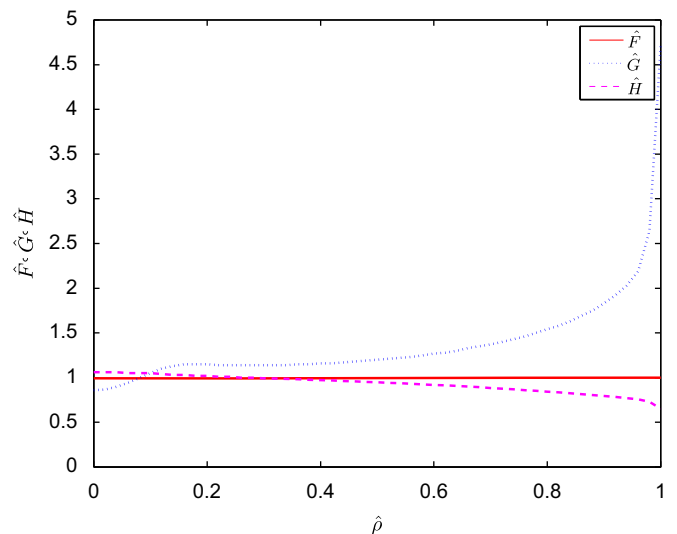


Fig. 3. Geometric factors  $\hat{F}$ ,  $\hat{G}$ , and  $\hat{H}$ .

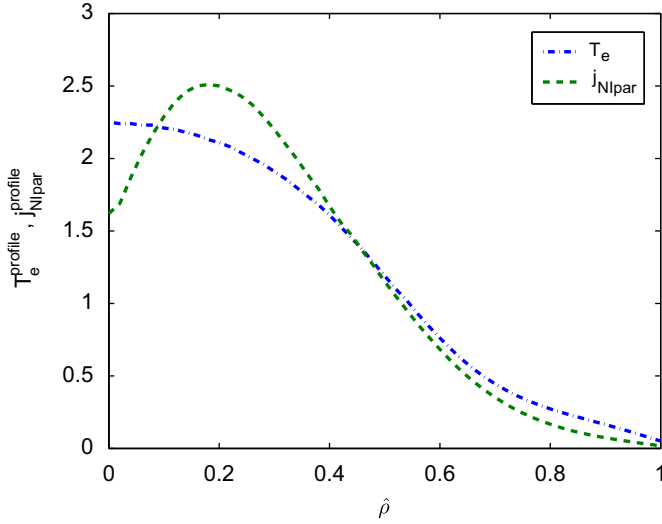


Fig. 4. Temperature ( $T_e^{\text{profile}}$ ), and non-inductive toroidal current density ( $j_{\text{NIpar}}^{\text{profile}}(\hat{\rho})$ ) profiles.

The non-inductive toroidal current density  $\langle \bar{j}_{\text{NI}} \cdot \bar{B} \rangle / B_{\phi,0}$  is assumed to follow:

$$\frac{\langle \bar{j}_{\text{NI}} \cdot \bar{B} \rangle}{B_{\phi,0}} = k_{\text{NIpar}} j_{\text{NIpar}}^{\text{profile}}(\hat{\rho}) \frac{I(t)^{1/2} P_{\text{tot}}(t)^{5/4}}{\bar{n}(t)^{3/2}}, \quad (4)$$

where  $j_{\text{NIpar}}^{\text{profile}}$  is given in Fig. 4, and  $k_{\text{NIpar}} = 1.2139 \times 10^{18} \text{ m}^{-9/2} \text{ A}^{-1/2} \text{ W}^{-5/4}$ .

The resistivity  $\eta$  scales with the temperature  $T_e$  as

$$\eta(\hat{\rho}, t) = \frac{k_{\text{eff}} Z_{\text{eff}}}{T_e^{3/2}(\hat{\rho}, t)}, \quad (5)$$

where  $Z_{\text{eff}} = 1.5$ , and  $k_{\text{eff}} = 4.2702 \times 10^{-8} \Omega \text{ m keV}^{3/2}$ .

The current density that flows toroidally around the tokamak,  $\langle \bar{j} \cdot \bar{B} / B_{\phi,0} \rangle$ , and whose profile must be controlled, is related to spatial derivative of the poloidal magnetic flux,

$$\frac{\langle \bar{j} \cdot \bar{B} \rangle}{B_{\phi,0}} = \frac{1}{\mu_0 \rho_b^2 \hat{r}^2 \hat{H} \hat{\rho}} \frac{\partial}{\partial \hat{\rho}} \left( \hat{\rho} \hat{r} \hat{G} \hat{H} \frac{1}{R_0} \frac{\partial \psi}{\partial \hat{\rho}} \right). \quad (6)$$

### 3. Control problem description

The control objective, as well as the dynamic models for current profile evolution, depend on the phases of the discharge (Fig. 2). During “Phase I” the control goal is to drive the current profile from any arbitrary initial condition to a prescribed target or desirable profile at some time  $T \in [T_1, T_2]$  in the flat-top phase of the total current  $I(t)$  evolution. However, since the available actuators during “Phase I” differ from those used during “Phase II”, and are constrained, the prescribed target profile is not an equilibrium profile during “Phase I”. During “Phase II” the control goal is to regulate the current profile using as little control effort as possible because the actuators are not only limited in power but also in energy. For this reason, the goal during “Phase I” is to set up an initial profile for “Phase II” as close as possible to its desirable profile.

This paper focuses on “Phase I”. It is important to note that although  $T_1$  and  $T_2$  can be adjusted as functions of the properties of the system, such as time scale and efficiency of the actuators, due to the nonlinearities of the system and the constraint of the actuators there is no guarantee that the target profile can indeed be reached within the time window  $[T_1, T_2]$ . Therefore, an optimal

control problem must be solved, where control laws  $I(t)$ ,  $P_{\text{tot}}(t)$ , and  $\bar{n}(t)$  are sought to minimize the cost functional

$$J = \sqrt{\min_{t_j} (J^*(t_j))}, \quad (7)$$

where  $t_j$  are discrete points in time equally spaced within the interval  $[T_1, T_2]$ , e.g.,  $t(j) = T_1 = 1.2 \text{ s}, 1.3 \text{ s}, 1.4 \text{ s}, \dots, T_2 = 2.4 \text{ s}$  for  $j = 1, 2, 3, \dots, 13$ , and  $J^*(t_j)$  is given by

$$J^*(t_j) = \frac{1}{N} \sum_{i=1}^N (\iota(\hat{\rho}_i, t_j) - \iota^{\text{des}}(\hat{\rho}_i))^2, \quad (8)$$

where  $N$  is the number of discrete points in space within the interval  $[0, 1]$  for the normalized radius,  $\iota(\hat{\rho}, t)$  denotes the rotational transform, and  $\iota^{\text{des}}(\hat{\rho})$  represents its desired value.

The safety factor  $q$  is a measure of the pitch of the helicoidal magnetic field lines lying on the magnetic surfaces, i.e., of the relation between the toroidal and poloidal components of the helicoidal magnetic field lines,  $q = d\Phi/d\psi$ . In a tokamak discharge, the toroidal field (TF) coils are operated so as to produce an approximately constant toroidal field. Thus, the  $q$  profile is considered in most cases to be a function of the variable poloidal field, or equivalently of the poloidal flux, i.e.,  $q = q(\psi)$ . When the plasma shape is controlled at steady-state equilibrium, the poloidal field (PF) coil currents are nearly constant. Therefore, changes in the poloidal field, and therefore in the poloidal flux  $\psi$ , are dominated by changes in the spatial distribution of the plasma toroidal current density (the current profile). Through this chain of dependencies, it can be seen that the safety factor  $q$  profile depends on the current profile (and vice versa). Thus, many physicists speak interchangeably of the current profile and the  $q$ -profile. Another quantity related to  $q$  is its inverse, known as the rotational transform  $\iota(\psi) = 1/q(\psi)$ . It can be shown that  $\iota(\psi)$  is proportional to the total current inside the flux surface represented by the poloidal flux value  $\psi$ . For this reason, the cost functional (7) has been defined in terms of this variable. The safety factor  $q$  and the rotational transform  $\iota$  are related and defined as

$$\iota(\rho, t) = \frac{1}{q(\rho, t)} = \frac{\partial \psi(\rho, t)}{\partial \Phi}. \quad (9)$$

The constant relationship between  $\Phi$  and  $\rho$ ,  $\rho = \sqrt{\Phi/\pi B_{\phi,0}}$ , and the definition of the normalized radius allow us to rewrite (9) as

$$\iota(\hat{\rho}, t) = \frac{\partial \psi}{\partial \hat{\rho}} \frac{1}{B_{\phi,0} \rho_b^2 \hat{\rho}}. \quad (10)$$

“Phase I” can be roughly divided into two phases, the ramp-up phase and the flattop phase. During the ramp-up phase, the three actuators  $I(t)$ ,  $\bar{n}(t)$  and  $P_{\text{tot}}(t)$  are assumed available for current profile control, whereas during part of the flattop phase ( $t > T_1$ )  $I(t)$  and  $\bar{n}(t)$  are chosen to be fixed although modulation of these variables is possible. In addition to these specific constraints during the flattop phase, the absolute values, and sometimes the derivatives in time, of the control variables must be within some specific limits during the whole “Phase I”. The physical ranges for  $I(t)$ ,  $\bar{n}(t)$  and  $P_{\text{tot}}(t)$  are given by

$$\begin{cases} 0 \leq I(t) \leq I_{\text{max}}, \\ \left| \frac{dI(t)}{dt} \right| \leq dI_{\text{max}}, \end{cases} \quad (11)$$

$$\begin{cases} I(\text{MA}) \leq \frac{\bar{n}(t)}{10^{19}} \leq 5I(\text{MA}), \\ dn_{\text{min}} \leq d\bar{n}(t)/dt \leq dn_{\text{max}}, \end{cases} \quad (12)$$

$$P_{\text{min}} \leq P_{\text{tot}}(t) \leq P_{\text{max}}. \quad (13)$$

The lower and upper limits for the line average density in (12) are set to prevent density instabilities and disruptions. The upper limit is approximately half of the Greenwald limit (Wesson, 2004). To accurately reproduce experimental discharges, constraints for  $I(t)$  and  $\bar{n}(t)$  are added at the initial time of “Phase I”, i.e.,

$$\begin{cases} I(t=0s) = I_0, \\ \bar{n}(t=0s) = \bar{n}_0. \end{cases} \quad (14)$$

In addition, a value of the total current  $I(t)$  is prescribed for the flattop phase, i.e.,

$$I(t \geq T_1) = I_{target}. \quad (15)$$

In summary, the optimal control problem (7) must be solved taking into account that (i) during the ramp-up phase ( $0 \leq t \leq T_1$ ) the three actuators can be manipulated while obeying the physical constraints (11)–(14), (ii) during the flattop phase  $I(t)$  is constrained by (15), and  $\bar{n}(t)$  must be equal to  $\bar{n}(T_1)$ . Control laws for  $I(t)$ ,  $\bar{n}(t)$  and  $P_{tot}(t)$  for  $t \in [0, T]$  are sought to make  $i(\hat{\rho}, T)$  as close as possible to the prescribed target profile  $i^{des}(\hat{\rho})$  at some time  $T \in [T_1, T_2]$ .

#### 4. Closed-loop optimal control

In this section, a closed-loop, receding-horizon, optimal controller based on extremum-seeking or nonlinear-programming optimization frameworks is presented.

##### 4.1. Receding horizon control (RHC)

The optimal control problem defined in Section 3 is assumed to be solved at time  $t=0$  by determining the actuator trajectory for  $t \geq 0$  that minimizes the cost function (7). The situation at time  $t=t_i$  illustrated in Fig. 5 is considered. If there were no disturbances and no model-plant mismatch, the actual profile would be identical to the profile predicted by the dynamic model. In this case, the application of the actuator trajectory found at time  $t=0$  for all time  $t \geq t_i$  would drive the actual profile to its target value (dashed curve) at time  $T$ . However, this is not a realistic assumption. The actual profile at time  $t_i$  will be in general different from the predicted value. In this case, the continuous application of the actuator trajectory found at time  $t=0$  will drive the actual profile to a final value that is different from the target

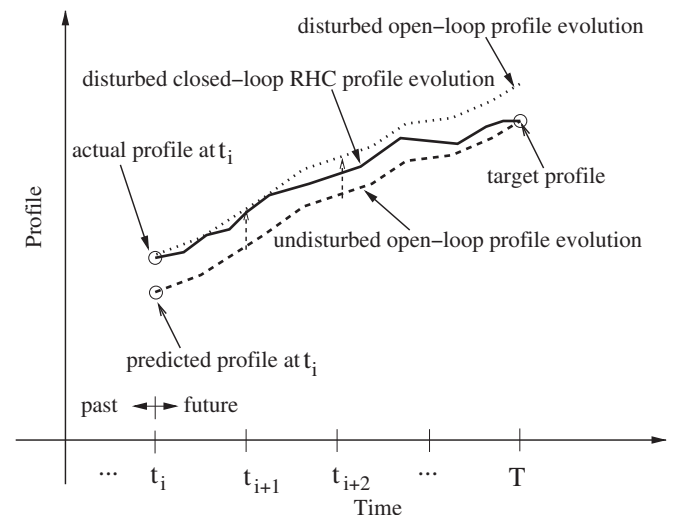


Fig. 5. Receding horizon control (RHC) scheme.

value (dotted curve). In order to incorporate some feedback mechanism, a receding horizon control strategy could be implemented, where a finite-horizon open-loop optimal control problem subject to system dynamics and actuator constraints is solved on-line at each time  $t_i$  and a new actuator trajectory resulting from the optimization process is implemented. The optimal control problem solved at each time  $t_i$  uses a direct measurement of the actual profile as initial condition, which provides indeed the desired feedback mechanism. This implies that the actuator trajectory computed at time  $t_i$ , for  $t_i \leq t \leq T$ , is implemented only until time  $t_{i+1}$  when the next measurement becomes available. This receding horizon control strategy will drive the actual profile to its target value at time  $T$  even in the presence of disturbances and plant-model mismatch (solid curve).

Fig. 6 shows the structure of the receding horizon control algorithm proposed in this work to address the current profile optimal control problem. Provided a measurement of  $\psi(\hat{\rho}, t_i)$ , the PDE model (1) and (2) uses it as its initial condition and predicts the output  $i(\hat{\rho}, t)$  for  $t_i \leq t \leq T$ , which can be in turn employed to compute  $i(\hat{\rho}, T)$  using (9). By minimizing the cost function (7) using an extremum seeking (Ou et al., 2008) or a nonlinear programming (Xu et al., 2010) approach, the optimal control inputs are obtained for  $t_i \leq t \leq T$ . Since the optimization procedure is carried out in the interval  $[t_i, t_{i+1}]$  to provide enough computational time, the control inputs actually implemented on the system during this time interval are considered as actuator constraints during the optimization. The calculated optimal control inputs are implemented on the actual system only for  $t_{i+1} \leq t \leq t_{i+2}$ , while a new optimization is carried out based on the measurement of  $\psi(\hat{\rho}, t_{i+1})$ .

##### 4.2. Open-loop optimization

Extremum-seeking (Ou et al., 2008) and nonlinear-programming (Xu et al., 2010) algorithms are considered in this work for the solution of the optimal control problem (7) at each sampling time  $t_i$ , for  $i = 1, \dots, N$ . As illustrated in Fig. 7, by parameterizing the control laws for  $I(t)$ ,  $P_{tot}(t)$  and  $\bar{n}(t)$  in terms of a set of discrete-time values denoted by  $\theta$ ,  $\theta$  is iteratively tuned to make the quadratic error between  $i(\hat{\rho}, T)$  and the prescribed target profile  $i^{des}(\hat{\rho})$  as small as possible at some time  $T \in [T_1, T_2]$ , i.e., to solve the optimization problem defined by

$$\min_{\theta} J(\theta), \quad (16)$$

with  $J$  defined in (7). The number of parameters used to represent the control laws is indeed a choice of the designer, and at the same time a tradeoff between the accuracy of the parameterization and the convergence speed of the optimization algorithm.

The control parameters  $\theta$  are changed or tuned after each simulated plasma “discharge”. In a simulation environment,

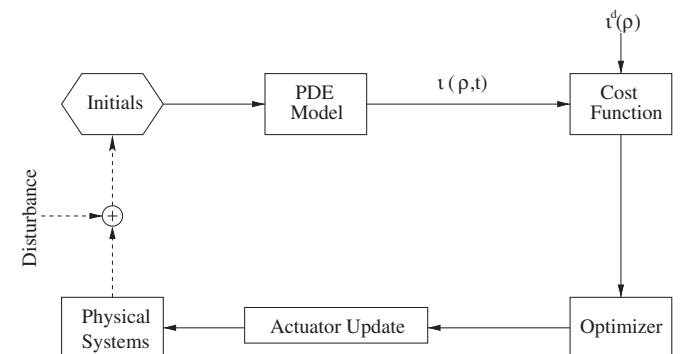


Fig. 6. Closed-loop receding-horizon control strategy.

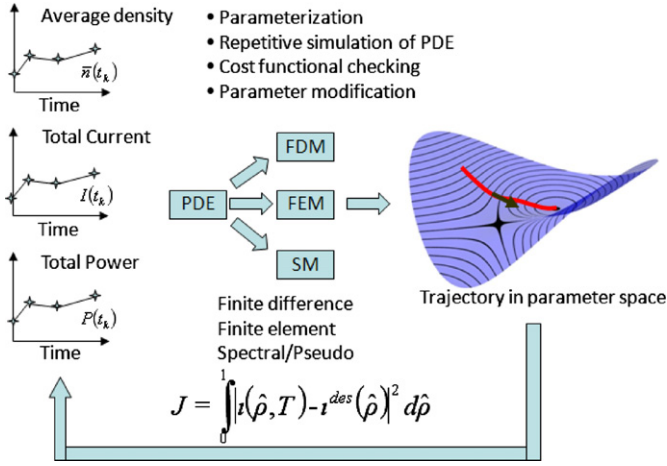


Fig. 7. Optimization approach.

a “discharge” is represented by the integration of the PDE Eqs. (1) and (2) in the interval  $[t_i, T_2]$  by using numerical methods such as finite differences, finite elements or pseudo-spectrum. In each iteration of the optimization procedure,  $\theta(k)$  is used to reconstruct the time evolution of the three physical actuators  $I(t)$ ,  $\bar{n}(t)$  and  $P_{tot}(t)$  in this time interval. At each sampling time  $t_i$ , the vector parameter  $\theta$  has 10 components given by

$$\theta = [I(t_i^1), I(t_i^2), P_{tot}(t_i), P_{tot}(t_i^{P1}), P_{tot}(t_i^{P2}), P_{tot}(T_1), \bar{n}(t_i^{n1}), \bar{n}(t_i^{n2}), \bar{n}(t_i^{n3}), \bar{n}(T_1)], \quad (17)$$

where  $t_i < t_i^1, t_i^2, t_i^{P1}, t_i^{P2}, t_i^{n1}, t_i^{n2}, t_i^{n3} < T_1$ . As an example, the optimal polynomial interpolation problem defined for the reconstruction of the plasma current  $I(t)$  is stated below. Similar optimization problems are defined for the other control laws. By taking into account that  $I(t_i) = I_i$  is fixed by the outcome of the optimization at  $t = t_{i-1}$ , or by the initial condition ( $I(0s) = I_0$ ), and  $I(T_1) = I_{target}$ , and using polynomial curve fitting for the points  $I(t_i), I(t_{i+1}), I(t_{i+2}), I(T_1)$ , the profile for  $I(t)$  for  $t \in [t_i, T_1]$  can be reconstructed. In addition,  $I(t) = I_{target}$  for  $t \in (T_1, T_2]$ . The plasma current is written as a polynomial in time  $t$ , i.e.,

$$I(t) = \sum_{j=0}^{n_{fit}^i} x_j t^{n_{fit}^i - j}, \quad (18)$$

where  $n_{fit}^i$  denotes the order of the fitting polynomial and  $x_j$ , for  $j=0, \dots, n_{fit}^i$ , are its coefficients. Recalling that  $\theta_1$  and  $\theta_2$  represent the value of plasma current determined by the optimization algorithm at  $t = t_i^1$  and  $t = t_i^2$ , respectively, the coefficient vector is denoted as  $x = [x_0 \dots x_{n_{fit}^i}]$  and the cost functional is defined as

$$J_{fit}^i(x) = (I(t = t_i^1) - \theta_1)^2 + (I(t = t_i^2) - \theta_2)^2. \quad (19)$$

The optimal polynomial interpolation problem can be written then as

$$\min_x J_{fit}^i(x), \quad (20)$$

subject to the following constraints:

$$\begin{cases} I(t = t_i) = I_i, \\ I(t = T_1) = I_{target}, \\ |dI(t_k)/dt| \leq dI_{max}, \\ 0 < I(t_k) < I_{max}, \end{cases} \quad (21)$$

where  $t_k = t_i, (t_i + (T_1 - t_i)/10), (t_i + 2(T_1 - t_i)/10), \dots, (t_i + 9(T_1 - t_i)/10), T_1$ .

After reconstructing the control laws for  $I(t)$ ,  $P_{tot}(t)$  and  $\bar{n}(t)$ , the PDE Eqs. (1) and (2) is integrated and the simulated profile  $i(\hat{\rho}, t)$

is obtained. The output of the nonlinear static map,  $J(k) = J(\theta(k))$ , is then calculated by evaluating (7) and used to compute  $\theta(k+1)$  according to the optimization procedure illustrated in Fig. 7.

### 4.3. Receding horizon algorithm

The combination of the receding horizon control framework and the extremum seeking or nonlinear programming optimization techniques can be summarized as follows.

Select the tolerance  $\varepsilon > 0$  and the maximum number of iterations for the extremum-seeking or nonlinear-programming optimal control algorithm, load the desirable  $i^{des}(\hat{\rho})$  profile data, and perform the following steps:

1. Define  $t_i = t_0$ . Implement off-line-computed actuator trajectories  $u(t)$ , for  $t \geq t_i = t_0$ . Provide the actual poloidal magnetic flux profile  $\psi(\hat{\rho}, t_i = t_0)$  as initial condition for the PDE model.
2. Compute the predicted  $i(\hat{\rho}, T)$  from the output  $\psi(\hat{\rho}, t)$ , for  $t \geq t_i$ , obtained from the PDE model.
3. Compute cost function (7). If it is less than  $\varepsilon$ , go to step 5.
4. Adjust the parameters  $\theta$  (i.e.  $u(t)$ ) in the optimization algorithm until the cost function is less than  $\varepsilon$  or the maximum number of iterations is reached. Use the actuator trajectories implemented for  $[t_i, t_i + \Delta t]$  as constraints.
5. Implement the calculated actuator trajectories on the actual system for  $[t_i + \Delta t, t_i + 2\Delta t]$ , move the control horizon one sampling interval  $\Delta t$  ahead, measure the output of the actual system  $\psi(\hat{\rho}, t_i + \Delta t)$ , make  $t_i = t_i + \Delta t$ , and go to step 2.

### 5. Simulation results

In this section, simulation results showing the effectiveness of the closed-loop, receding-horizon control scheme in a disturbance rejection problem are presented for three different cases. In the simulation study, the magnetic flux diffusion PDE is reduced to a set of ODEs by carrying out a second-order-accurate spatial discretization based on a fixed set of nodes (Skeel & Berzins, 1990). In the first case, the optimization problem (7) is solved in open loop for a nominal initial profile. The limitations of the open-loop controller to cope with disturbances in the initial profile is manifested in the second case, where a disturbed initial profile is considered. Finally, in the third case, the performance of the closed-loop controller is analyzed when the same disturbed initial profile is considered. All the open-loop optimizations carried out in the simulation study presented in this section are based on extremum-seeking (Ou et al., 2008).

In these simulations, the time interval  $[0, T_2 = 2.4 \text{ s}]$  is considered. The current  $I(t)$  is reconstructed in the interval  $[t_i, T_1 = 1.2 \text{ s}]$  using polynomial interpolation to fit the discrete points  $I(t = t_i) = I_i \text{ MA}$ ,  $I(t = t_i^1) = \theta_1$ ,  $I(t = t_i^2) = \theta_2$ ,  $I(t \geq T_1 = 1.2 \text{ s}) = 1.18774 \text{ MA}$ . The value of  $I_i$  is fixed by the outcome of the optimization at  $t = t_{i-1}$ , or by the initial condition  $I(0s) = I_0$ , where  $I_0 = 0.7092 \text{ MA}$ . The constraints for  $I(t)$  are as follows:

$$\begin{cases} 0 \leq I(t) \leq 1.19141 \text{ MA}, \\ \left| \frac{dI(t)}{dt} \right| \leq 2 \text{ MA/s}. \end{cases} \quad (22)$$

In each interval  $[t_i, T_1 = 1.2 \text{ s}]$ , the total power  $P_{tot}(t)$  is reconstructed using polynomial interpolation to fit the discrete points  $P_{tot}(t = t_i) = \theta_3$ ,  $P_{tot}(t = t_i^{P1}) = \theta_4$ ,  $P_{tot}(t = t_i^{P2}) = \theta_5$ ,  $P_{tot}(t = T_1 = 1.2 \text{ s}) = \theta_6$ . For  $t > T_1 = 1.2 \text{ s}$ ,  $P_{tot}(t) = P_{tot}(T_1)$ . The additional constraint for  $P_{tot}(t)$  is given by

$$0 \leq P_{tot}(t) \leq 20 \text{ MW}. \quad (23)$$

The average density  $\bar{n}(t)$  is obtained by similar procedure in each interval  $[t_i, T_1 = 1.2 \text{ s}]$ , given the discrete points  $\bar{n}(t = t_i) = \bar{n}_i$ ,  $\bar{n}(t = t_1^{n1}) = \theta_7$ ,  $\bar{n}(t = t_1^{n2}) = \theta_8$ ,  $\bar{n}(t = t_1^{n3}) = \theta_9$ ,  $\bar{n}(t = T_1 = 1.2 \text{ s}) = \theta_{10}$ . For  $t > T_1 = 1.2 \text{ s}$ ,  $\bar{n}(t) = \bar{n}(T_1)$ . The value of  $\bar{n}_i$  is fixed by the outcome of the optimization at  $t = t_{i-1}$ , or by the initial condition  $\bar{n}(0 \text{ s}) = \bar{n}_0$ , where  $\bar{n}_0 = 2.0 \times 10^{19} \text{ m}^{-3}$ . The constraints for  $\bar{n}(t)$  are written as

$$\begin{cases} I(t)(\text{MA}) \leq \frac{\bar{n}(t)}{10^{19}}(\text{m}^{-3}) \leq 5I(t)(\text{MA}), \\ -1.7 \times 10^{19} \text{ m}^{-3} \text{ s}^{-1} \leq d\bar{n}(t)/dt \leq 3 \times 10^{19} \text{ m}^{-3} \text{ s}^{-1}. \end{cases} \quad (24)$$

The initial values for  $\theta$  are arbitrarily chosen as

$$\theta_{int} = [0.938721 \text{ MA}, 1.15723 \text{ MA}, 1.15723 \text{ MW}, 0.860596 \text{ MW}, 1.09253 \text{ MW}, 1.09253 \times 2 \text{ MW}, 1 \times 10^{19} \text{ m}^{-3}, 2 \times 10^{19} \text{ m}^{-3}, 3 \times 10^{19} \text{ m}^{-3}, 4 \times 10^{19} \text{ m}^{-3}].$$

### 5.1. Open-loop control

The nominal initial poloidal flux  $\psi$  considered in this simulation case is shown in Fig. 8 (solid blue line). The target or desirable  $\iota$  profile is shown in Fig. 10 (solid green line). The optimal control problem is solved in open loop. After less than 100 iterations, a minimum is achieved. The corresponding normalized cost function is  $J = 0.0285$ . Fig. 10 shows the resulting matching (blue dashed-dotted line). The corresponding time evolutions for the three actuators are shown in Fig. 9.

The initial poloidal flux profile is now changed while the open-loop controller shown in Fig. 9 is still used. Fig. 8 shows the disturbed initial poloidal flux profile considered in this case (green dashed-dotted line), and compares it with the nominal initial poloidal flux profile. The cost function results now  $J = 0.0404$ . Fig. 10 shows the difference between the obtained  $\iota$  profile (dotted black line) and the desirable  $\iota$  profile. As expected, the matching is worsened due to the disturbance in the initial poloidal flux profile.

### 5.2. Closed-loop control (disturbance rejection)

In the third simulation case, the closed-loop, receding-horizon control strategy is implemented. At  $t = t_0 = 0$ , the “measured”  $\psi$  profile is the disturbed initial poloidal flux profile, shown in Fig. 8, and the open-loop actuator trajectories are used for control. After  $\Delta t = 0.1 \text{ s}$ , the control input is updated with the result of the optimizer. The procedure is repeated until  $t = T_1 = 1.2 \text{ s}$ . From that instant the control input is kept unmodified until the end of the considered time interval

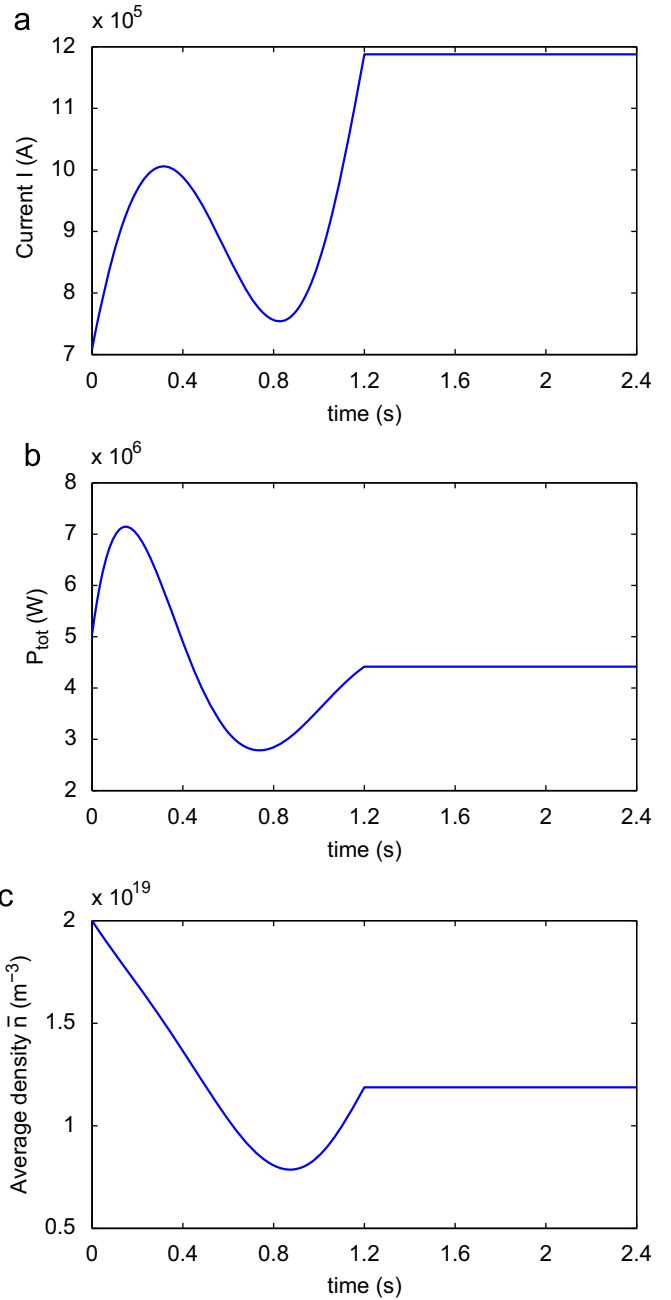


Fig. 9. Open-loop, extremum-seeking, optimal control.

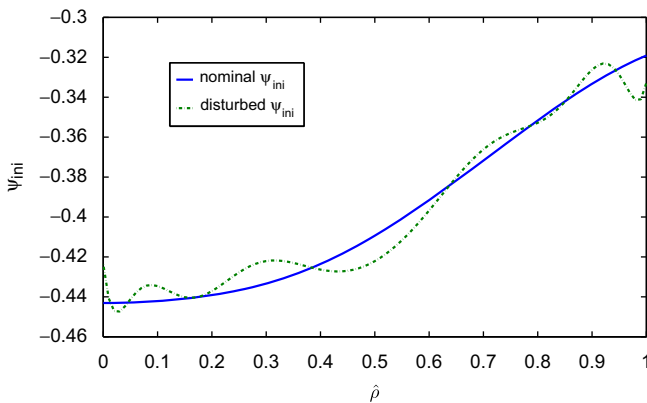


Fig. 8. Comparison of initial  $\psi$  profiles.

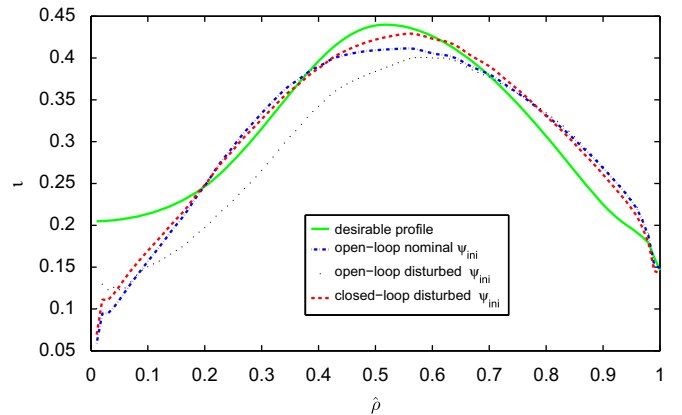


Fig. 10. Comparison of  $\iota$  matching.

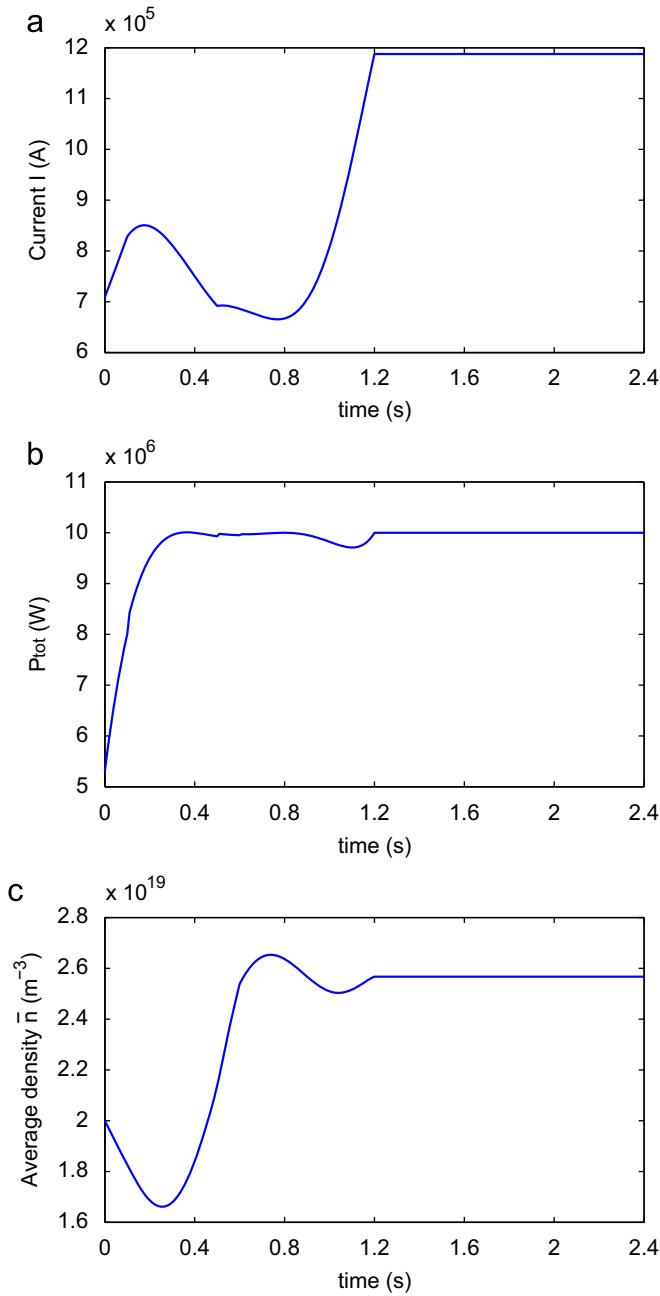


Fig. 11. Closed-loop, extremum-seeking, receding-horizon optimal control.

at  $T_2=2.4$ . For each optimization started at  $t = (k-1) \times 0.1$  s for  $k=1, \dots, 11$ , the  $\psi$  profile is measured and incorporated into the optimization procedure. At time  $t = k \times 0.1$  s for  $k=1, \dots, 11$ , the actuator trajectories are updated using the solution to the stated optimal control problem provided by the optimizer.

For the closed-loop controller, the achieved matching shown in Fig. 10 (dashed red line) gives a cost function  $J=0.0246$ . Fig. 11 shows the closed-loop control actuator trajectories. Fig. 10 compares the matching of the target  $i$  by open- and closed-loop controllers. The closed-loop approach provides a better matching as it is illustrated by the results in Table 1.

### 5.3. Implementation issues

For a practical implementation of a receding horizon controller, the computational burden is as critical as the optimization

**Table 1**  
Comparison of open-loop and closed-loop control results.

Cost function			
	Undisturbed open-loop	Disturbed open-loop	Disturbed closed-loop
$J$	0.0285	0.0404	0.0246

**Table 2**  
Comparison of cost-function value and run-time as a function of the number of iterations and  $\Delta\hat{\rho}$  when  $\Delta t = 0.1$  s.

Number of iterations	$\Delta\hat{\rho} = 0.01$		$\Delta\hat{\rho} = 0.02$	
	Cost function	Run-time (s)	Cost function	Run-time (s)
1	0.0407	$T_1$	0.0471	$0.49T_1$
10	0.0298	$T_2=08.08T_1$	0.0319	$0.50T_2$
20	0.0254	$T_3=16.40T_1$	0.0260	$0.51T_3$
50	0.0246	$T_4=41.67T_1$	0.0258	$0.51T_4$

quality. These two competing objectives show a clear tradeoff; by reducing the optimization iterations the computational burden is decreased at the price of a lower optimization quality. A study is carried out in this subsection to assess how these two factors depend on a few critical implementation variables such as: (i) the number of iterations in each optimization; (ii) the time interval  $\Delta t$  in the receding horizon control algorithm, and (iii) the spatial interval  $\Delta\hat{\rho}$  in the numerical integration of the PDE system.

A series of simulations is presented in Tables 2 and 3. The label “number of iterations” refers to the number of iterations in a single optimization process, the label “cost function” denotes the value defined in Eq. (7), and the label “run-time” represents the time required to carry out the complete optimization over the 0–2.4 s interval.

Table 2 compares cost-function values and run-times as a function of the number of iterations when  $\Delta t = 0.1$  s is kept fixed. Results for both  $\Delta\hat{\rho} = 0.01$  and 0.02 are presented. By looking at the results for the  $\Delta\hat{\rho} = 0.01$  case it is possible to conclude first that the run-time is directly proportional to the number of iterations, and second that the cost-function value decreases as the number of iterations increases. However, this last relationship is not linear (see how small is the improvement in the cost-function value when the number of iterations is increased from 20 to 50), indicating the existence of an optimal value for the cost-function value vs. number of iterations tradeoff. By comparing the  $\Delta\hat{\rho} = 0.01$  and 0.02 cases it is possible to note that while the cost-function value is kept approximately constant, i.e., the quality of the optimization is preserved, the run-time is inversely proportional to the spatial discretization step  $\Delta\hat{\rho}$  used for the simulation of the PDE system. This suggests that the implementation of model reduction techniques for the approximation of the infinite-dimensional PDE model by a low-order finite-dimensional ODE (ordinary differential equation) model has the potential of dramatically reducing the computational burden of the proposed receding horizon control scheme.

Table 3 compares cost-function values and run-times as a function of the number of iterations when  $\Delta\hat{\rho} = 0.02$  is kept fixed. Results are presented for three values of the receding-horizon-control time interval  $\Delta t$ . The study of the behavior of the cost-function value when  $\Delta t$  is increased keeping the ratio  $n_{iter}/\Delta t$  constant ( $n_{iter}$  denotes the number of iterations) is of interest. The increase of the number of iterations  $n_{iter}$  proportionally to the time interval  $\Delta t$  ensures that the computational burden is kept approximately constant. The cases  $\Delta t = 0.1$  s/ $n_{iter} = 10$ ,

**Table 3**  
Comparison of cost-function value and run-time as a function of the number of iterations and  $\Delta t$  when  $\Delta\hat{p} = 0.02$ .

Number of iterations	$\Delta t = 0.01$ s		$\Delta t = 0.02$ s		$\Delta t = 0.04$ s	
	Cost function	Run-time (s)	Cost function	Run-time (s)	Cost function	Run-time (s)
1	0.0471	0.49T <sub>1</sub>	0.0419	0.29T <sub>1</sub>	0.0395	0.18T <sub>1</sub>
10	0.0319	4.05T <sub>1</sub>	0.0309	2.31T <sub>1</sub>	0.0325	1.47T <sub>1</sub>
20	0.0260	8.36T <sub>1</sub>	0.0260	4.92T <sub>1</sub>	0.0291	2.89T <sub>1</sub>
40	0.0260	17.08T <sub>1</sub>	0.0250	9.23T <sub>1</sub>	0.0275	5.68T <sub>1</sub>

$\Delta t = 0.2$  s/ $n_{iter} = 20$ , and  $\Delta t = 0.4$  s/ $n_{iter} = 40$  are considered. While the run-time is kept very similar, the cost-function values indicate that there may be an optimal  $\Delta t/n_{iter}$  pair for a given constant ratio  $n_{iter}/\Delta t$ . Too much feedback with little optimization or little feedback with too much optimization represent the limiting cases, which are clearly not optimal.

## 6. Conclusions and future work

A simplified dynamic model describing the evolution of the poloidal flux, and therefore the  $\iota$  profile, during the inductive phase of the discharge has been introduced. Using this model, a closed-loop, receding-horizon, optimal controller based on extremum-seeking and nonlinear-programming techniques has been proposed to match a desired  $\iota$  profile within a predefined time window during the flattop phase of the tokamak discharge. The extremum-seeking and nonlinear-programming procedures have shown in previous work to be effective in dealing with an optimal control problem defined for a PDE system subject to many actuator constraints, and where not only interior and boundary control but also diffusivity control are considered. The proposed controller satisfactorily rejects disturbances due to its feedback nature.

The proposed closed-loop receding-horizon scheme shows potential for implementation in long-discharge tokamaks such as ITER. Future work towards reducing the computation time includes strategies such as: (i) implementation of model reduction techniques to approximate the infinite-dimensional PDE model by a low-order finite-dimensional ODE model, (ii) approximation of the solution of the nonlinear optimal control problem by successive computation of linear optimal control problems, and (iii) combination of off-line feedforward and on-line feedback control strategies, where the feedback controller is intended to track an off-line-computed trajectory in the presence of disturbances and plant-model mismatches. Finally, the experimental validation of this type of controller in long-discharge superconducting tokamaks (Tore Supra, EAST, KSTAR) is also part of the future work in this area.

## Acknowledgements

This work has been supported in part by the NSF CAREER Award Program (ECCS-0645086), and the U.S. Department of Energy (DE-FG02-09ER55064).

## References

Ariyur, K., & Krstic, M. (2003). *Real-time optimization by extremum seeking feedback*. Wiley.  
 Barana, O., Mazon, D., Laborde, L., & Turco, F. (2007). Feedback control of the lower hybrid power deposition profile on tore supra. *Plasma Physics and Controlled Fusion*, 49, 947–967.  
 Bleijs, L., & Kothare, M. (2005). Reduced order distributed boundary control of thermal transients in microsystems. *IEEE Transactions on Control Systems Technology*, 13(6), 853–867.

Borrelli, F., Falcone, P., & Vecchio, C. D. (2007). Event-based receding horizon control for two-stage multi-product production plants. *Control Engineering Practice*, 15(12), 1556–1568.  
 Challis, C. (2004). The use of internal transport barriers in tokamak plasmas. *Plasma Physics and Controlled Fusion*, 46(12B), B23–B40.  
 Christofides, P. (2001). *Nonlinear and robust control of PDE systems*. Birkhauser.  
 Connor, J., Fukuda, T., Garbet, X., Gormezano, C., Mukhovatov, V., & Wakatani, M. (2004). A review of internal transport barrier physics for steady-state operation of tokamaks. *Nuclear Fusion*, 44(4), R1–R49.  
 Dubljevic, S., El-Farra, N. H., Mhaskar, P., & Christofides, P. D. (2006). Predictive control of parabolic PDEs with state and control constraints. *International Journal of Robust and Nonlinear Control*, 16, 749–772.  
 Ferron, J., Gohil, P., Greenfield, C., Lohr, J., Luce, T., & Makowski, M., et al. (2006). Feedback control of the safety factor profile evolution during formation of an advanced tokamak discharge. *Nuclear Fusion*, 46(10), L13.  
 Findeisen, R., & Allgower, F. (2002). An introduction to nonlinear model predictive control. In *Proceedings of the 21st Benelux meeting on systems and control*.  
 Freidberg, J. P. (1987). *Ideal magnetohydrodynamics*. New York: Plenum Press.  
 Irizarry-Rivera, R., & Seideer, W. D. (1997). Model-predictive control of the Czochralski crystallization process. Part I. Conduction-dominated melt. *Journal of Crystal Growth*, 178, 593–611.  
 Keviczky, T., & Balas, G. J. (2006). Receding horizon control of an f-16 aircraft: A comparative study. *Control Engineering Practice*, 14(9), 1023–1033.  
 Kim, K. B., Yoon, T.-W., & Kwon, W. H. (2001). Receding horizon guidance laws for constrained missiles with autopilot lags. *Control Engineering Practice*, 9(10), 1107–1115.  
 Krstic, M., & Smyshlyayev, A. (2008). *Boundary control of PDEs: A short course on backstepping designs*. SIAM.  
 Laborde, L., Mazon, D., Moreau, D., Murari, A., Felton, R., & Zabeo, L., et al. (2005). A model-based technique for integrated real-time profile control in the JET tokamak. *Plasma Physics and Controlled Fusion*, 47(1), 155–183.  
 Leuer, J. (1995). Fusion nature's fundamental energy source. Workbook.pdf. <<http://fusioned.gat.com/classroom.html>>, March.  
 Marjanovic, O., & Lennox, B. (2004). Infinite horizon model predictive control with no terminal constraint. *Computers and Chemical Engineering*, 28, 2605–2610.  
 Mayne, D., & Michalska, H. (1990). Receding horizon control of nonlinear systems. *IEEE Transactions on Automatic Control*, 35, 814–823.  
 Mayne, D., Rawlings, J., Rao, C., & Sckaert, P. (2000). Constrained model predictive control: Stability and optimality. *Automatica*, 26, 789–814.  
 Moreau, D., Crisanti, F., Litaudon, X., Mazon, D., Vries, P. D., & Felton, R., et al. (2003). Real-time control of the q-profile in JET for steady state advanced tokamak operation. *Nuclear Fusion*, 43(9), 870–882.  
 Moreau, D., Mazon, D., Ariola, M., Tommasi, G. D., Laborde, L., & Piccolo, F., et al. (2008). A two-time-scale dynamic-model approach for magnetic and kinetic profile control in advanced tokamak scenarios on JET. *Nuclear Fusion*, 48, 106001.  
 Nocedal, J., & Wright, S. J. (2006). *Numerical optimization* (2nd ed.). New York: Springer.  
 Ou, Y., Luce, T., Schuster, E., Ferron, J., Walker, M., & Xu, C., et al. (2007). Towards model-based current profile control at DIII-D. *Fusion Engineering and Design*, 82, 1153–1160.  
 Ou, Y., Xu, C., Schuster, E., Luce, T., Ferron, J., & Walker, M., et al. (2008). Extremum-seeking open-loop control of plasma current profile at the DIII-D tokamak. *Plasma Physics and Controlled Fusion*, 50, 115001.  
 Patwardhan, A., Wright, G., & Edgar, T. (1992). Nonlinear model-predictive control of distributed-parameter systems. *Chemical Engineering Science*, 47, 721–735.  
 Pironti, A., & Walker, M. (2005). Fusion, tokamaks, and plasma control. *IEEE Control System Magazine*, 25(5), 30–43.  
 Richalet, J. (1993). Industrial applications of model based predictive control. *Automatica*, 29, 1251–1274.  
 Schuster, E., & Ariola, M. (2006). The role of controls in nuclear fusion. In *Proceedings of the 45th IEEE conference on decision and control*.  
 Skeel, R. D., & Berzins, M. (1990). A method for the spatial discretization of parabolic equations in one space variable. *SIAM Journal on Scientific and Statistical Computing*, 11, 1–32.  
 Suzuki, T., Isayama, A., Ide, S., Fujita, T., Oikawa, T., Sakata, S., et al. (2005). Recent RF experiments and application of RF waves to real-time control of safety factor profile in JT-60U. In *AIP conference* (Vol. 787, pp. 279–286).  
 Taylor, T. (1997). Physics of advanced tokamaks. *Plasma Physics and Controlled Fusion*, 39(Suppl. 12B), B47–B73.  
 Toure, Y., Biston, J., & Gilles, G. (1994). Modeling of a distributed parameter process with a variable boundary: Application to its control. *Chemical Engineering Science*, 49, 61–73.

- van Straten, G., van Willigenburg, L. G., & Tap, R. F. (2002). The significance of crop co-states for receding horizon optimal control of greenhouse climate. *Control Engineering Practice*, 10(6), 625–632.
- Walker, M., Humphreys, D., Mazon, D., Okabayashi, D. M., Osborne, T., & Schuster, E. (2006). Emerging applications in tokamak plasma control. Control solutions for next-generation tokamaks. *IEEE Control System Magazine*, 26(2), 35–63.
- Wesson, J. (2004). *Tokamaks* (3rd ed.). Oxford: Clarendon Press.
- Wijnands, T., et al. (1997). Feedback control of the current profile on Tore Supra. *Nuclear Fusion*, 37(6), 777.
- Xu, C., Ou, Y., Dalessio, J., Schuster, E., Luce, T., & Ferron, J., et al. (2010). Ramp-up phase current profile control of tokamak plasmas via nonlinear programming. *IEEE Transactions on Plasma Science*, 38(2), 163–173.